Spectroelectrochemical Analysis of the Intervalence Band in Mixed-Valence Di- and Tetranuclear Ru Complexes by the Flow-Through Method

Masa-aki Haga,*,† Md. Meser Ali,‡ Hiroyasu Sato,‡ Hideaki Monjushiro,† Koichi Nozaki,§ and Kenji Kano||

Coordination Chemistry Laboratory, Institute for Molecular Science, Myoudaiji, Okazaki, Aichi 444, Japan, Department of Chemistry for Materials, Faculty of Engineering, Mie University, Kamihama-cho, Tsu, Mie, 514, Japan, Graduate School of Science, Osaka University, Machikaneyama, Toyonaka, Osaka 560, Japan, and Department of Agricultural Chemistry, Kyoto University, Kitashirakawaoiwake, Sakyou-ku, Kyoto 606, Japan

Received June 27, 1997

Introduction

There is an upsurge of interest in the redox chemistry of polynuclear complexes in connection with multielectron transfer reagents and photochemical energy collectors. Complexes that show multielectron redox reactions include linear metal polymers, supramolecular species, and dendrimers. The dendritic tetranuclear complexes, shown in Scheme 1, can be regarded as a core for a dendrimer and the simplest unit of the Bethe lattice.[1] This type of tetranuclear complexes has two different coordination environments around the metal ions: one is the central metal ion, and the other is made up of the three peripheral metal ones. Few papers have dealt with the detailed redox chemistry of dendritic tetranuclear complexes,[2,3] although many synthetic works of tetranuclear Ru complexes with bridging ligands have been reported.[4−10] Therefore, we report here the detailed oxidation chemistry of dendritic Ru complexes including an analysis of the near infrared absorption spectra of mixed-valence states.

Redox chemistry of this type of complexes strongly depends not only on donor/acceptor property of a bridging ligand but also on ancillary ligands around Ru ions. Furthermore, the strength of metal−metal interaction can be mainly determined by the bridging ligand. In the case of weak metal−metal interaction mediated through bridging ligand and three peripheral metal complexes having the same coordination environments, two oxidation patterns have been so far reported in the ligand-bridged dendritic tetranuclear complexes. The first pattern (A) exhibits that the central one-electron oxidation occurs first, followed by three peripheral metal oxidations at almost identical potentials. The second pattern (B) is that three peripheral oxidations at first, followed by the central one-electron oxidation. When the three-electron process is analyzed more precisely, this process can be generally separated into three closely spaced one-electron processes, arising from the weak electrostatic interactions and/or the statistic factors. Thus, three mixed-valence states can be considered in oxidation processes for the dendritic tetranuclear complex. Since potential separations among these three processes are generally small, a selective oxidation could not be achieved and even the one-electron oxidized species might be easily disproportionated into the original and two-electron oxidized species. Therefore, accurate determination of absorption spectra for the mixed-valence complexes should be determined by considering the comproportionation equilibria. Richardson and Taube[11] have reported the electrochemical method for analyzing the near-infrared spectra in weakly coupled dinuclear complexes based on the digital simulation and spectrophotometric titration method for dinuclear Ru complexes. Launay et al. reported the determination of the intervalence bands in Ru ammine complexes bridged by various π-conjugated organic systems[12] and oxidized aromatic polyamines by using the typical redox titration with a chemical oxidant coupled with bulk electrolysis.[13]

Recently, we have reported the synthesis and properties of dendritic tetranuclear Ru and Os 2,2′-bipyridine complexes bridged by 2,2′-bis(1-benzimidazo-2-yl)-4,4′-bipyridine.[14−16]

Scheme 1. Structure of Dendritic Ru Tetranuclear Complex in the Present Study

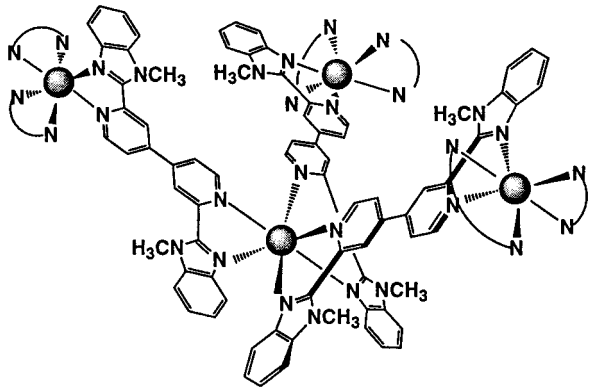

* Corresponding author. E-mail address: mhaga@chem.chuo-u.ac.jp.
† Institute for Molecular Science.
‡ Mie University.
§ Osaka University.
|| Kyoto University.

(1) Stauffer, D.; Aharonu, A. *Introduction to Percolation Theory*; Stauffer, D., Aharonu, A., Eds.; Taylor and Francis: London, 1992; pp 26.
(2) Aoki, K.; Chen, J.; Haga, M. *J. Electroanal. Chem.* **1995**, *396*, 309−316.
(3) Roffia, S.; Marcaccio, M.; Paradisi, C.; Paolucci, F.; Balzani, V.; Denti, G.; Serroni, S.; Campagna, S. *Inorg. Chem.* **1993**, *32*, 3003−3009.
(4) Rillema, D. P.; Callahan, R. W.; Mack, K. B. *Inorg. Chem.* **1982**, *21*, 2589−2596.
(5) Denti, G.; Campagna, S.; Sabatino, L.; Serroni, S.; Ciano, M.; Balzani, V. *Inorg. Chem.* **1990**, *29*, 4750−4758.
(6) Denti, G.; Serroni, S.; Campagna, S.; Ricevuto, V.; Balzani, V. *Inorg. Chim. Acta* **1991**, *182*, 127−129.
(7) Denti, G.; Campagna, S.; Serroni, S.; Ciano, M.; Balzani, V. *J. Am. Chem. Soc.* **1992**, *114*, 2944−2950.
(8) Wacholtz, W. E.; Auerbach, R. A.; Schmehl, R. H. *Inorg. Chem.* **1987**, *26*, 2989−2994.
(9) Campagna, S.; Denti, G.; Serroni, S.; Ciano, M.; Balzani, V. *Inorg. Chem.* **1991**, *30*, 3728−3732.
(10) Belser, P.; von Zelewsky, A.; Frank, M.; Seel, C.; Vogtle, F.; De Cola, L.; Barigelletti, F.; Balzani, V. *J. Am. Chem. Soc.* **1993**, *115*, 4076−4086.
(11) Richardson, D. E.; Taube, H. *Inorg. Chem.* **1981**, *20*, 1278−1285.
(12) Ribou, A.-C.; Launay, J.-P.; Takahashi, K.; Nihira, T.; Tarutani, S.; Spangler, C. W. *Inorg. Chem.* **1994**, *33*, 1325−1329.
(13) Bonvoisin, J.; Launay, J.-P.; Van der Auweraer, M.; De Schryver, F. C. *J. Phys. Chem.* **1994**, *98*, 5052−5057.
(14) Haga, M.; Ali, M. M.; Arakawa, R. *Angew. Chem., Int. Ed. Engl.* **1996**, *35*, 76.
(15) Arakawa, R.; Matsuo, T.; Nozaki, K.; Ohno, T.; Haga, M. *Inorg. Chem.* **1995**, *34*, 2464−2467.
(16) Arakawa, R.; Mastsubayashi, G.; Ohashi, N.; Furuuchi, S.; Matsuo, T.; Ali, M. M.; Haga, M. *J. Mass. Spectrom.* **1996**, *31*, 861.

S0020-1669(97)00794-5 CCC: $15.00
Published on Web 04/17/1998

Scheme 2. Stepwise One-Electron Oxidations of Dendritic Ru Tetranuclear Complex for the Oxidation Pattern (A): The Circles Stand for the Ru Components

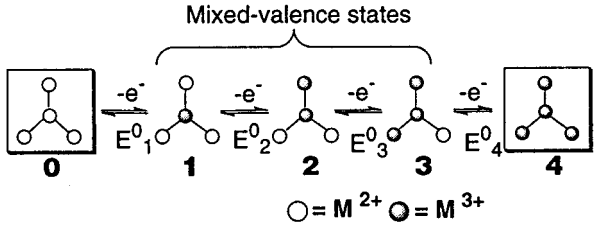

The oxidation of these dendritic complexes takes place by the pattern (A) process, having four closely spaced one-electron processes as shown in Scheme 2. During the progress of electrochemical oxidation, a characteristic near-infrared (NIR) band was observed, which can be assigned to intervalence charge transfer (IT) transition within the mixed-valence state. In order to reconstruct the corrected absorption spectra of each mixed-valence complex, we have developed a new method based on the combination of a CV digital simulation and a flow-through electrolysis in this paper. This method will be widely applicable for the analysis of intervalence charge-transfer band in polynuclear complexes.

Experimental Section

The Ru complexes, $[(bpy)_2Ru(bptb)Ru(bpy)_2]^{4+}$ and $[\{(bpy)_2Ru(dmbbbpy)\}_3Ru]^{8+}$ (bpy = 2,2′-bipyridine; bptb = 2,6-bis(2-pyridyl)-2,2′:6,2′-thiazolo[4,5-*d*]benzothiazole dmbbbpy = 2,2′-bis(1-methylbenzimidazo-2-yl)-4,4′-bipyridine), were prepared followed by the reported procedures.[15,17] The flow-through electrolysis was performed with the same flow-through cell as reported previously.[18] In the present study, the redox potential for the ferrocenium/ferrocene is +0.09 V vs $Ag/AgNO_3$ (0.01 M in CH_3CN with 0.1 M $TBABF_4$), abbreviated as Ag^+/Ag.

Calculation of IT Band of the Redox Intermediates. We consider a sequential four-step one-electron-transfer mechanism for the redox reaction of a dendritic tetranuclear complex, of which the standard (macroscopic) redox potentials of each redox step are designated as E_1°, E_2°, E_3°, and E_4°, respectively, as shown in Scheme 2. The mass balance of the redox species **j** ($j = 0-4$) can be written by

$$C_t = \sum_{j=0}^{4} C_j \tag{1}$$

where C_t and C_j are the total concentration and the concentration of the redox species **j** of the tetranuclear complex. Under redox equilibrium conditions at a solution potential of E, the concentration ratio between two redox species **j** and **j**−**1** can be expressed by the Nernst equation.

$$\frac{C_j}{C_{j-1}} = \exp\left[\frac{F(E - E_j^\circ)}{RT}\right] \qquad (j = 1-4) \tag{2}$$

The apparent j-electron redox potential (e_j°) can be defined as

$$e_j^\circ = \frac{\sum_{k=1}^{j} E_k^\circ}{j} \qquad (j = 1-4) \tag{3}$$

Combination of eqs 2 and 3 leads to

$$C_j = C_0 \exp\left[\frac{jF(E - e_j^\circ)}{RT}\right] \qquad (j = 1-4) \tag{4}$$

By substituting eq 4 into eq 1, we can obtain

$$C_t = C_0 \sum_{j=0}^{4} \eta_j \tag{5}$$

where $\eta_0 = 1$ and $\eta_j = \exp[jF(E - e_j^\circ)/RT]$ for $j = 1-4$. Thus C_j can be expressed as a function of η_j (or E).

$$C_j = \frac{\eta_j C_t}{\sum_{k=0}^{4} \eta_k} \qquad (j = 0-4) \tag{6}$$

The value of absorbance (A_λ) for the mixture of redox species **0**−**4** at a given wavelength (λ) can be written by eq 7.

$$A_\lambda = \sum_{j=0}^{4} \epsilon_{j,\lambda} C_j l \tag{7}$$

where $\epsilon_{j,\lambda}$ and l are the absorption coefficient of the species **j** and the light path length, respectively, although the redox intermediate species **1**, **2**, and **3** only are responsible for the IT band. By combining eqs 6 and 7, A_λ can be expressed as a function of η_j (or E).

$$A_\lambda = \frac{\sum_{j=0}^{4} \epsilon_{j,\lambda} \eta_j C_t l}{\sum_{j=0}^{4} \eta_j} \tag{8}$$

In principle, experimental A_λ vs the column electrode potential (E_c) curves might be subjected to nonlinear regression analysis based eq 8 to evaluate $\epsilon_{j,\lambda}$ and E_j° with knowledge of C_t and l. Under the present column electrolytic conditions, however, the ohmic drop would be expected and the reversibility of the electrode process was not completely confirmed, that is, the true (or effective) value of E during the column electrolysis might be less negative than E_c. Then we attempted to evaluate E as follows.

The experimental value of the steady-sate current (i) at a given E_c in a column electrolysis provides the apparent number of electrons (n) for the oxidation as defined by

$$n = n_t \frac{i}{i_{lim}} \tag{9}$$

where n_t is the total number of electrons ($n_t = 4$ for tetranuclear complexes) and i_{lim} is the limiting oxidation current observed at sufficiently positive E_c under given conditions. The physical meaning of n is given by eq 10 as a function of E.

$$n = \frac{\sum_{j=0}^{4} jC_j}{C_t} = \frac{\sum_{j=0}^{4} j\eta_j}{\sum_{j=0}^{4} \eta_j} \tag{10}$$

Therefore, plots of A_λ against n obtained by the column-electrolytic spectroelectrochemical technique can be theoretically analyzed on the basis of eqs 8 and 10 using E as a medium valuable. The nonlinear least-squares analysis of A_λ vs n plots allows simultaneous determination of $\epsilon_{j,\lambda}$, and E_j°, in principle. For the nonlinear least-squares analysis, a

(17) Haga, M.; Ali, M. M.; Koseki, S.; Yoshimura, A.; Nozaki, K.; Ohno, T. *Inorg. Chim. Acta* **1994**, *226*, 17−24.
(18) Ohno, T.; Nozaki, K.; Haga, M. *Inorg. Chem.* **1992**, *31*, 548−555.

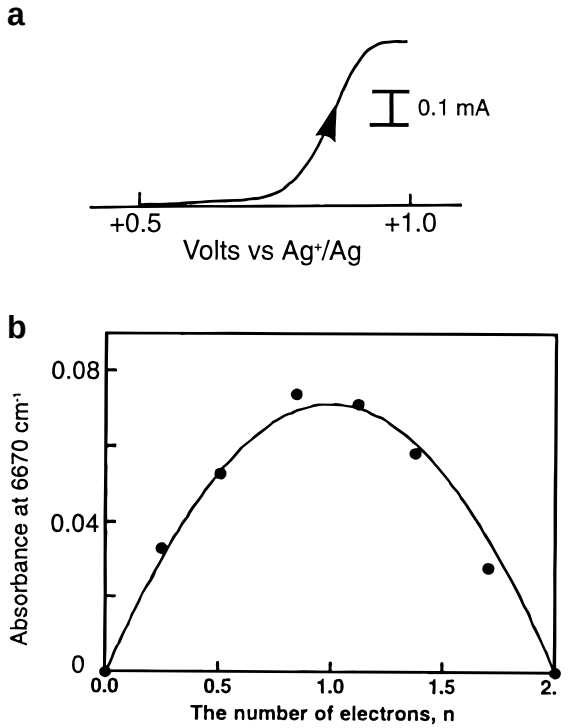

Figure 1. (a) Steady-state voltammogram of $[(bpy)_2Ru(bptb)Ru(bpy)_2]^{4+}$ in CH_3CN at the flow-through electrolysis condition: flow rate = 500 μL/min; scan rate = 10 mV/s. (b) Plot of absorbance at 6670 cm^{-1} (1500 nm) vs the number of electrons, *n*, obtained from the current ratio for the complex, $[(bpy)_2Ru(bptb)Ru(bpy)_2]^{4+}$ (7.65×10^{-4} M).

dumping Gauss−Newton method[19] was used and the program was written on Turbo Pascal. A similar experimental and analytical procedure was repeated at various λ in the region interested, in which a set of the identical values of E_j° ($j = 1-4$) was employed. Thus, one can predict and reconstruct absorption spectra of the intermediate redox species **1**, **2**, and **3**.

In nonlinear least-squares analysis for the tetranuclear complex, however, seven adjustable parameters, $\epsilon_{j,\lambda}$ ($j = 1-3$) and E_j° ($j = 1-4$), are required, $\epsilon_{o,\lambda}$ and $\epsilon_{4,\lambda}$ being determined experimentally and treated as fixed parameters. Such nonlinear regression with many adjustable parameters might give rise to an unstable conversion or a large standard deviation. To reduce the number of the adjustable parameters, E_j° ($j = 1-4$) may be independently evaluated by digital simulation-coupled nonlinear regression analysis of the reversible cyclic voltammogram of the complex[20] and used as fixed parameters in the analysis of A_λ vs *n* plots. In this way, we can reconstruct the corrected near-infrared spectra for the mixed-valence states with an experimental error of 10%.

Results and Discussion

By using this dinuclear $[(bpy)_2Ru(bptb)Ru(bpy)_2]^{4+}$ system, we have checked the effectiveness of our flow-through method by comparison with conventional spectroelectrochemical methods. Figure 1a shows the steady-state hydrodynamic voltammogram of $[(bpy)_2Ru(bptb)Ru(bpy)_2]^{4+}$ in CH_3CN. From the hydrodynamic voltammogram, the *n* value at a given column electrode potential (E_c) was evaluated according to eq 9. Plots of A_{6670} (absorbance at 6670 cm^{-1} (1500 nm)) vs *n* for $[(bpy)_2Ru(bptb)Ru(bpy)_2]^{4+}$ in CH_3CN are shown in Figure 1b. The A_{6670} vs *n* plots were analyzed on the basis of eqs 8 and 10, in which $\epsilon_{1,6670}$ as well as E_1° and E_2° were used as adjustable parameters. The result of the nonlinear curve-fitting was as follows: $\epsilon_{1,6670} = 160$ M^{-1} cm^{-1}, $E_1^\circ = 0.865$ V, and $E_2^\circ = 0.904$ V vs Ag^+/Ag, and the regression curve is also attached as a solid line in Figure 1b. We have previously reported the calculated intervalence band of $[(bpy)_2Ru(bptb)Ru(bpy)_2]^{5+}$ in CH_3CN.[18] The same result for the comproportionation constant value and IT band was obtained when the oxidative titration by cerium(IV) sulfate as a oxidant, which indicates effectiveness of our flow-through method in dinuclear mixed-valent complexes.

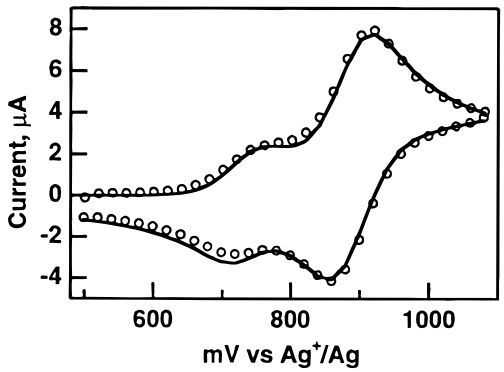

Figure 2. Cyclic voltammogram of $[\{(bpy)_2Ru(dmbbbpy)\}_3Ru]^{8+}$ in CH_3CN at the platinum working electrode: scan rate = 50 mV/s; digital simulation result shown as a solid line.

Figure 2 shows an example of the cyclic voltammogram (CV) of tetranuclear Ru complex, $[\{(bpy)_2Ru(dmbbbpy)\}_3Ru]^{8+}$, in which small and large reversible waves are clearly separated. The total number of electrons (n_t) involved in the overall oxidation was confirmed to be four by controlled potential coulometry at +1.1 V vs Ag^+/Ag. Comparing this oxidation pattern with those of analogous complexes, the first small wave at a lower redox potential is ascribed to the oxidation reaction of the central Ru(II) ion and the second large wave to that of three peripheral Ru(II) ions, as shown in Scheme 2. The peak separations of anodic and cathodic waves were practically independent of the scan rate (υ) in the region from at least from 10 to 500 mV s^{-1}, guaranteeing the reversibility of the electrode process under the conditions. Thus, we performed digital simulation-coupled nonlinear regression analysis of the CV curves on the basis of the sequential four-step one-electron transfer mechanism. The resultant curve is also given in Figure 2 as a solid line. The observed CV curve was fairly well reproduced by the simulated one, and the four oxidation potentials have been evaluated as: $E_1^\circ = 0.732$ V, $E_2^\circ = 0.859$ V, $E_3^\circ = 0.888$ V, and $E_4^\circ = 0.918$ V vs Ag^+/Ag (with a diffusion coefficient of 2.5×10^{-6} cm^2 s^{-1}). E_1° is assigned to the central Ru ion and the others to the peripheral Ru(II) ions, as illustrated in Scheme 2.

In sequential four-step electron transfers, the disproportionation of the redox intermediates **j** into **j**−**1** and **j**+**1** must be considered (Scheme 3). The equilibrium constant (K_j) is written by eq 11.

$$K_j = \frac{C_{j-1}C_{j+1}}{C_j^2} = \exp\left[\frac{F(E_{j-1}^\circ - E_{j+1}^\circ)}{RT}\right] \quad (j = 1-3) \quad (11)$$

Substitution of E_1° and E_2° into eq 11 yields $K_1 = 0.0071$ at 25 °C. Therefore, the disproportionation of the species **1** is practically ignored in our case, while species **2** and **3** undergo disproportionation significantly, as judged from $K_2 = 0.32$ and $K_3 = 0.31$.

(19) Kowalik, J.; Osborne, M. R. *Methods in Unconstrained Optimization Problems*; Elesevier: Amsterdam, 1968.
(20) Kano, K.; Sugimoto, T.; Misaki, Y.; Enoki, T.; Hatakeyama, H.; Oka, H.; Hosotani, Y.; Yoshida, Z. *J. Phys. Chem.* **1994**, *98*, 252.

Scheme 3. Comproportionation Equilibria of Dendritic Ru Tetranuclear Complex

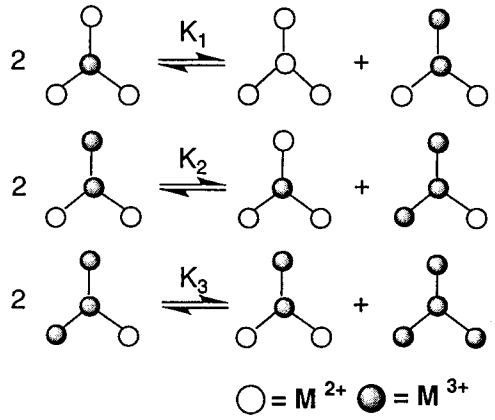

Scheme 4. Scrambling Equilibria in the Tetranuclear Ru Complex

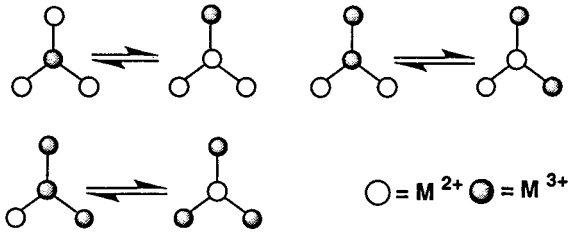

Considering the fact that E_1° is less positive by about 0.12−0.19 V than E_2°, E_3°, and E_4°, some scrambling equilibria as depicted in Scheme 4 are reasonably ignored. Thus, we focus our attention to the three sequential redox steps of the peripheral Ru ions by considering **1** as a starting material. When we assume that the identical three peripheral Ru ions are not interactive with each other, each step is progressively more difficult due to the statistical factor, as pointed out by Bard and colleagues.[21] Therefore, E_j° values ($j = 2-4$) are written by eq 12.

$$E_j^\circ = E_{2-4}^\circ + \left(\frac{RT}{F}\right)\ln\left[\frac{j}{4-j}\right] \qquad (j = 2-4) \qquad (12)$$

where $E_{2-4}^\circ = (E_2^\circ + E_3^\circ + E_4^\circ)/3$. Equation 12 predicts that $E_3^\circ - E_2^\circ = E_4^\circ - E_3^\circ = 28.2$ mV at 25 °C, which is in good agreement with the simulation results: $E_3^\circ - E_2^\circ = 29$ mV and $E_4^\circ - E_3^\circ = 30$ mV. Thus, we can safely conclude that the three peripheral Ru moieties of the tetranuclear complex are noninteractive with each other.

Figure 3a shows a hydrodynamic voltammogram of the tetranuclear $[\{(bpy)_2Ru(dmbbbpy)\}_3Ru]^{8+}$ complex taken by the column-electrolytic method. The voltammogram exhibited a one-electron oxidation wave at about 0.75 V ascribed to the oxidation of **0** to **1**, followed by a three-electron redox wave of **1** to **4**. The steady-state current (i) reached the limiting value (i_{lim}) at column electrode potentials (E_c) more positive than ca. 1 V, where the complex is fully oxidized into **4**. The electrolyzed solution was collected and subjected to absorption spectroscopy in the near-infrared (NIR) region. A new NIR band around 7690 cm^{-1} (1300 nm) increased once for the partially oxidized solution and then decreased, indicating typical characteristics of intervalence band, although the fully oxidized complex **4** showed the foot of LMCT band in this region ($\epsilon_{4,7690} = 30$ M^{-1} cm^{-1}).

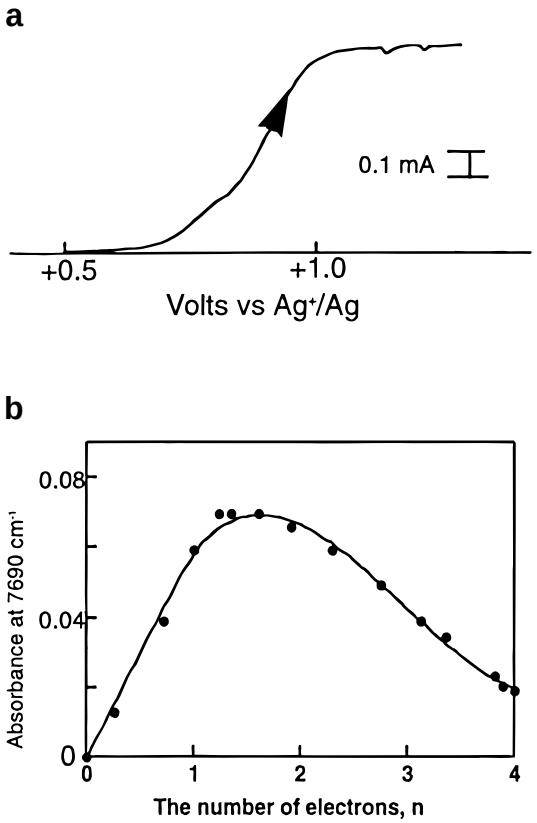

Figure 3. (a) Steady-state voltammogram of $[\{(bpy)_2Ru(dmbbbpy)\}_3Ru]^{8+}$ in CH_3CN at the flow-through electrolysis condition: flow rate = 500 μL/min; scan rate = 10 mV/s. (b) Plot of absorbance at 7690 cm^{-1} (1300 nm) vs the number of electrons, n, obtained from tthe current ratio for the complex, $[\{(bpy)_2Ru(dmbbbpy)\}_3Ru]^{8+}$ (2.3×10^{-4} M).

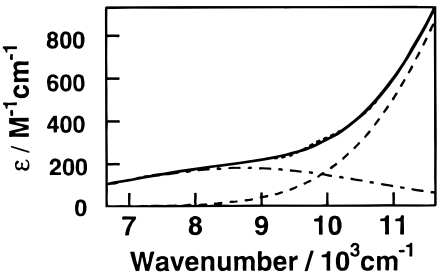

Figure 4. Corrected near-infrared spectra of two-electron oxidized $[\{(bpy)_2Ru(dmbbbpy)\}_3Ru]^{10+}$ obtained by the calculation; calculated spectrum (—) and the original spectra (···), together with the result of Gaussian spectral analysis for this regression spectrum (- - - and —·—).

The small first wave does not seem to be well resolved from the succeeding three-electron redox wave, as compared with the cyclic voltammogram in Figure 2. This could be ascribed to some ohmic drop. The situation indicates that A_λ vs n plots is superior to A_λ vs E_c plots in the thermodynamic analysis, where n is defined by $4i/i_{lim}$ (eq 9) and reflects the true (or effective) solution potential (E) (eqs 9 and 10).

Plots for A_{7690} vs n are shown in Figure 3b. Surprisingly, the NIR intensity maximum was situated at $n \sim 1.5$. The titration plots were simulated on the basis of eqs 8 and 10 using the E_j° values ($j = 1-4$) determined by the CV simulation and $\epsilon_{0,7690}$ and $\epsilon_{4,7690}$ described above. The corrected absorption spectra of the mixed valence species were reconstructed from

(21) Flanagan, J. B.; Margel, S.; Bard, A. J.; Anson, F. C. *J. Am. Chem. Soc.* **1978**, *100*, 4248.

$\epsilon_{j,\lambda}$ obtained at various NIR wavelengths, and Gaussian spectral analysis for these regression spectra has been performed: an example of the spectral anaylysis of two-electron oxidized $[\{(bpy)_2Ru(dmbbbpy)\}_3Ru]^{10+}$ is shown in Figure 4. The absorption coefficients at 8390 cm^{-1} for each mixed-valence species are obtained as follows: $\epsilon_1 = 120\ M^{-1}\ cm^{-1}$, $\epsilon_2 = 180\ M^{-1}\ cm^{-1}$, and $\epsilon_3 = 50\ M^{-1}$. The two-electron oxidized species **2** is found to exhibit the strongest NIR absorption, while the band energies for intervalence charge transfer and the LMCT band for mixed-valence complexes **1**−**3** stayed almost constant, $(8.39 \pm 0.5) \times 10^3$ and $(13.9 \pm 0.5) \times 10^3\ cm^{-1}$, respectively.

In conclusion, we have developed a convenient method using the flow-through electrolysis to obtain the NIR spectra of partially oxidized species. The combination of digital simulation analysis of a reversible CV curve and the electrochemical titration by using a flow-through cell leads to the complete spectral analysis of IT band for the partially oxidized species in the dendritic tetranuclear Ru complexes.

Acknowledgment. M.H. gratefully acknowledges financial support from the Ministry of Education, Science, Sports and Culture for a Grant-in-Aid for Scientific Research (Nos. 06804036 and 09440233).

Supporting Information Available: A figure showing the corrected near-infrared spectra for mixed-valence tetranuclear Ru species **0**−**4** (1 page). Ordering information is give on any current masthead page.

IC970794R